

# Optimization of a Close-Fitting Volume RF Coil for Brain Imaging at 6.5 mT Using Linear Programming

Sheng Shen , Zheng Xu , Neha Koonjoo, and Matthew S. Rosen 

**Abstract—Objective:** The use of a close-fitting roughly head-shaped volume coil for MRI (magnetic resonance imaging) has the merit of improving the filling factor and thus the SNR (signal-to-noise ratio) from the brain. However, the surface of the RF coil follows that of the head which makes it difficult to determine an optimal coil winding pattern. We describe here a new method to optimize a head-shaped RF coil with the objective of maximizing its SNR and RF-magnetic-field homogeneity for operation at ultra-low magnetic field (6.5 mT, 276 kHz). **Methods:** The approach consists of FEM (finite-element-method) simulation and linear programming based optimization. **Results:** We have implemented the optimization and further studied the relationship between the design requirements and the performance of the RF coil. Finally, we constructed an optimal RF coil and scanned both a head-shaped phantom and a human subject. **Conclusion:** The method we outline here provide new insight into the conductor layout needed for magnetic optimization of structurally complex coils, especially when tradeoffs between competing attributes (SNR and homogeneity in this case) must be made.

**Index Terms—**RF coil optimization, FEM simulation, linear programming, Ultra-low field MRI.

## I. INTRODUCTION

MRI TECHNOLOGY has demonstrated its irreplaceable role in clinical diagnosis and scientific research. MRI at

Manuscript received May 8, 2020; accepted June 9, 2020. Date of publication June 12, 2020; date of current version March 19, 2021. This work was supported in part by the National Natural Science Foundation of China under Grants 51677008 and 51707028, and in part by the Fundamental Research Funds for the Central Universities under Grants 2019CDYGYB001 and 2018CDJDDQ0017. M.S.R. acknowledges funding from the Advanced Research Projects Agency-Energy (ARPA-E), U.S. Department of Energy, under Award Number DE-AR0000823. (Corresponding authors: Zheng Xu; Matthew S. Rosen).

Sheng Shen is with the State Key Laboratory of Power Transmission Equipment and System Security and New Technology and also with the MGH/A.A. Martinos Center for Biomedical Imaging, Charlestown.

Zheng Xu is with the State Key Laboratory of Power Transmission Equipment and System Security and New Technology, Chongqing University, Chongqing 400044, China (e-mail: xuzheng@cqu.edu.cn).

Neha Koonjoo is with the MGH/A.A. Martinos Center for Biomedical Imaging, Charlestown and with the Department of Physics, Harvard University, and also with the Harvard Medical School.

Matthew S. Rosen is with the MGH/A.A. Martinos Center for Biomedical Imaging, Charlestown, MA 02129, USA, and with the Department of Physics, Harvard University, Cambridge, MA 02138 USA, and also with the Harvard Medical School, Boston, MA 02115 USA (e-mail: msrosen@mgh.harvard.edu).

Digital Object Identifier 10.1109/TBME.2020.3002077

ultra-low magnetic field (ULF) is an encouraging paradigm to enable lower cost and mobile scanners [1]–[3]. However, opportunities at ULF have been neglected for many years generally because of low SNR. In recent years, with the development of low noise hardware, computational approaches to MRI pulse sequences [4], and deep learning based approaches to image reconstruction [5], the performance of ultra-low-field MRI system has been improved. In 2015, Sarracanie *et al.* reported a 6.5 mT MRI scanner used for rapid brain imaging [6]; in 2019, Mäkinen *et al.* published work using a hybrid MEG-ULF MRI system [7].

In the presently described work, we focus on the design and optimization of a volume RF coil for human brain imaging at 6.5 mT. Volume RF conductor topologies used for brain imaging include birdcage, solenoid, and saddle coils. Birdcage coils have been exploited on most of the commercial MRI systems where it can generate a homogeneous transverse RF magnetic field, typically as a transmit/receive coil in quadrature mode. Since the RF magnetic field in this case is produced transverse to the coil cylinder axis, this geometry is only used for MRI system with cylindrical magnets [8]–[10]. The solenoid coil can generate a very homogenous axial RF magnetic field, however, in this case use of this geometry is typically limited to biplanar magnets [11], [12]. The saddle coil can generate a homogeneous RF magnetic field over a reasonable region of interest (ROI), and it has better geometric versatility allowing use on MRI scanners with either cylindrical or biplanar magnets. Nevertheless, saddle coils have low efficiency (defined as the RF magnetic field strength per unit current), which results in low intrinsic SNR [13], [14]. Beyond the RF coils described above, Helmholtz coils [15], phase array coils [16], transverse electro-magnetic (TEM) coils [17] and loop coils [18] all have utility in MRI, depending on the application.

The 6.5 mT ULF MRI scanner in our laboratory is based around a biplanar magnet [6], so we use modified solenoid coils for brain imaging on this scanner. As described in [6] and shown in Fig. 1, our previous work used RF coils closely fit to the shape of the head and uniformly wound on a helmet-shaped former to bring the RF coil close to the region of interest (ROI) without covering the face of patient. This improves the filling factor of the coil compared to an unmodified solenoid, and also prevents claustrophobia in the subject. The magnetic geometry matches the biplanar magnet well; compared to a modified saddle coil on a helmet-shaped surface, the solenoid produces a more homogeneous RF magnetic field at higher efficiency.

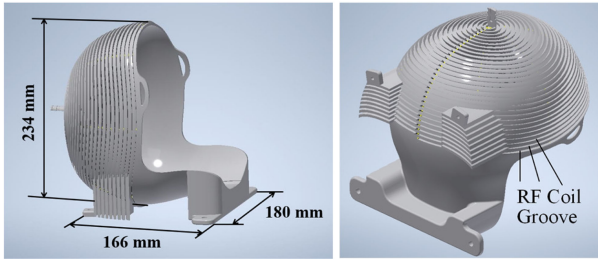


Fig. 1. Close-fitting brain helmet former with pre-determined evenly spaced wire grooves (shown here in two orientations).

We describe here work to further improve the performance of this modified solenoid RF coil using a novel method consisting of FEM simulation and linear programming to optimized the RF coil conductor pattern on the helmet-shaped surface. FEM simulation was used to calculate the magnetic field generated by the RF coil as well as the lumped parameters, inductance and resistance, of the RF coil. Based on the simulation results, we converted the coil pattern optimization to be a linear-programing problem. The mathematical model of linear programming was built to obtained a coil pattern with requirements of RF coil efficiency (defined as the average RF-magnetic-field strength of all target points in the imaged volume per unit current), and RF-magnetic-field homogeneity.

Linear programming is typically used when there is a known analytic expression to be optimized; there is a well-known linear-programing application in homogeneous magnet design, propose by Xu *et al.* in 1991 [19]. In our work, we combine the FEM simulation with linear programming to provide a new approach for the implementation of the optimization algorithm and electromagnetic design.

Once the optimization method was used to obtain a coil pattern that meets the design requirements, we analyzed the relationship between the design requirements and the performance of optimized RF coil. Based on the analysis, we designed an optimized RF coil and built a prototype. The prototype was used to scan head-shaped phantoms and human heads at 6.5 mT. The images obtained with the optimized RF coil were compared to that obtained by the uniformly wound spiral RF coil, reported in [7].

## II. METHOD

The optimization method consists of FEM simulation and liner programming. FEM simulation was used to calculate the magnetic field distribution of the head-shaped RF coil; the linear programming was used to obtain the RF coil conductor pattern consistent with our design requirements.

### A. FEM Simulation

As in [7], the close-fitting RF coil was wound on a helmet-shaped former, shown as Fig. 1. The evenly spaced grooves for the wire on the helmet were pre-determined. The imaging ROI with a shape similar to the head shown is seen in cyan and the wire groove are overlaid on the ROI, shown as Fig. 2(a).

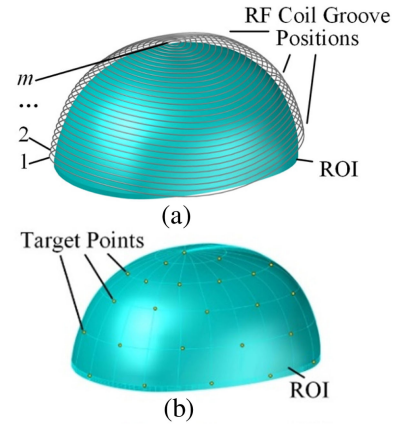


Fig. 2. Sketch of the mathematical model. (a) Wire groove positions on the surface of the helmet, where  $m$  is the index of wire groove positions; (b) ROI and the target points in the ROI.

To optimize the pattern of RF coil conductors, we first need to obtain the magnetic field distribution in ROI produced by each of the wire loops making up the coil. However, the shape of each loop is irregular which makes it difficult to deduce a concise analytic expression for the magnetic-field calculation. Thus, we introduce a FEM simulation to calculate the magnetic field distribution over the ROI. FEM simulation is a powerful tool for electromagnetic calculation and is usually implemented via commercial software, such as Ansys Maxwell (Ansys Inc.), CST (Dassault Systèmes SIMULIA Corp.) and COMSOL Multiphysics (COMSOL Inc.).

The RF magnetic field generated by the irregular loop at each position with a unit current was calculated by FEM simulation and the 3D model of loops for simulation was shown as Fig. 2(a), where the index of each loop is  $m$ ; the number of target points we chosen uniformly in ROI is  $n$ , shown as Fig. 2(b).

The magnetic field at each target point produced by unit current at all loop positions is denoted by a matrix  $A_{mn}$ . The magnetic field in the ROI was then calculated by:

$$B1 = A_{mn} \cdot I_m \quad (1)$$

Where,  $I_m$  is the vector which denotes the number of turns at each RF coil groove position, and  $B1$  is the RF magnetic field at the target points in ROI.

### B. Linear Programing

Besides the magnetic field calculation, we also quantified the performance of the RF coil in order to include it in the optimization problem. The performance parameters of RF coil include the SNR of RF coil, and the homogeneity of RF magnetic field.

The SNR of RF coil was defined as [20]:

$$SNR_0 = \frac{\sqrt{2}B1_0}{i \cdot \sqrt{R}} \quad (2)$$

Where,  $B1_0$ , the so-called effective RF magnetic field, is a component of RF magnetic field that is perpendicular to the direction of the static magnetic field of MRI system;  $R$  is the

resistance of RF coil;  $i$  is the current in the RF coil. However, in this optimization, the RF magnetic field was evaluated by  $B1_{av}$  which is the average of the effective RF magnetic field at all target points in ROI. Moreover, since we assume the RF coil is powered by a unit current, the SNR of RF coil simplifies to:

$$SNR = \frac{\sqrt{2}B1_{av}}{\sqrt{R}} \quad (3)$$

According to (3), if  $B1_{av}$  is fixed, then the SNR is only affected by the resistance of RF coil; the smaller the resistance, the higher the SNR. However, the SNR of RF coil is not the only parameter to be considered in RF coil optimization; the inductively detected signal received by RF coil has a frequency bandwidth which requires that the passband of RF coil be no narrower than the bandwidth of NMR signal. In the presence of frequency encoding, this is essential.

The passband of a RF coil is calculated as:

$$BW = \frac{f_0}{Q} \quad (4)$$

Where,  $f_0$  is the Larmor frequency of MRI system, and  $Q$  is the quality factor of RF coil, which may be calculated:

$$Q = \frac{\omega L}{R} \quad (5)$$

Where,  $\omega$  is the angular frequency corresponding to the Larmor frequency of MRI scanner;  $L$  is the inductance of RF coil.

In the MR imaging experiment, the bandwidth of the NMR signal is determined by the strength of the readout magnetic gradient (mT/m) over the FOV (m) being imaged. Therefore, for a given scanner with an imaging bandwidth (determined from the product of the maximum gradient strength with the FOV), in order to avoid attenuating the signal near the edges of the FOV, the maximum  $Q$  of the RF coil is calculated by (4). According to (3), (4) and (5), to improve the SNR of RF coil and for a fixed bandwidth, we should reduce the resistance and inductance of RF coil on the same time.

The resistance of the RF coil is affected by the conductivity of wire material, wire structure (e.g., solid, stranded, or litz wire), and the role of proximity- and eddy current effects. To first approximation, we look at the DC resistance which is proportion to the length of wire used to wind the RF coil. The inductance of a solenoid coil ( $L_s$ ) is calculated as (6) [21]:

$$L_s = \mu_0 \frac{N^2 A}{l} = \mu_0 \frac{\pi N^2 \sigma^2}{l} \quad (6)$$

where  $\mu_0$  is the permeability of air,  $N$  is the number of turns,  $A$  is the cross-section area of solenoid;  $\sigma$  is the radius of the cross-section;  $l$  is the length of the solenoid. Fig. 3 is the sketch of a solenoid.

According to (6), the inductance of a solenoid is proportional to the square of the number of turns  $N$ , and square of the radius of the cross-section  $\sigma$ . From this we note that the inductance of the coil increases as the total length of the wire is increased.

Based on the above, the objective of maximizing the SNR of RF coil can be thought of as a search for a coil winding pattern which can generate a specific  $B1_{av}$  using the least wire. This objective was expressed as equation (7) and (8). Where,  $B1_r$ ,

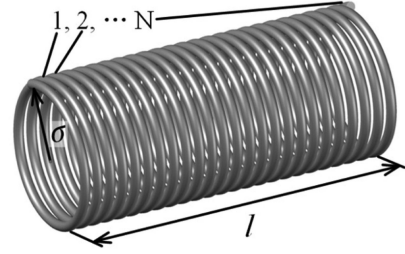


Fig. 3. Sketch of a solenoid of length  $l$  and number of turns  $N$ .

denotes the desired  $B1_{av}$  ( $B1_r$  is column vector, in which the element is  $B1_r$ ).  $Len$  denotes the length of the wire wound on the RF coil,  $Len_m$  is a matrix which denotes the length of each groove shown in Fig. 2(a).

$$Len = Len_m \cdot I_m \quad (7)$$

$$\frac{1}{n} \sum_{i=1}^n Amn \cdot I_m = B1_r \quad (8)$$

The elements in vector  $I_m$  are integer; the maximum value is 6, which is determined by the volume of each RF coil groove. With the requirement of integer solution, there may be no solution for (8) with a specific  $B1_r$ , thus, equation (8) was modified as following:

$$\left| \frac{\frac{1}{n} \sum_{i=1}^n Amn \cdot I_m - B1_r}{B1_r} \right| \leq \delta_0 \quad (9)$$

Where,  $\delta_0$  is a constant, and  $0.01 < \delta_0 < 0.05$ . Inequation (9) allows the average RF magnetic field of optimized RF coil be around the  $B1_r$ .

Another performance parameter of RF coil when used for imaging is the homogeneity of RF magnetic field; it is quantified by the maximum error, denoted by  $\delta$ , between the magnetic flux density at target points and  $B1_r$ , which is expressed as:

$$\left| \frac{Amn \cdot I_m - B1_r}{B1_r} \right| \times 100\% = \delta \quad (10)$$

Based on the analysis above, we have built a linear-programing model to determine the number of coil turns in each RF coil groove position with required RF-magnetic-field strength and homogeneity in ROI, expressed as following:

Minimization:

$$Len = Len_m \cdot I_m$$

Subject to:

$$\begin{cases} \left| \frac{\frac{1}{n} \sum_{i=1}^n (Amn \cdot I_m) - B1_r}{B1_r} \right| \leq \delta_0 \\ \left| \frac{Amn \cdot I_m - B1_r}{B1_r} \right| \times 100\% \leq \delta_1 \\ I_m = 0, 1, \dots, 6 \end{cases} \quad (11)$$

Where,  $\delta_1$  is the required maximum RF magnetic field error ( $\delta$ ) in the optimization.

This linear-programing problem, shown in (11), was solved by the function `intlinprog` in MATLAB (The MathWorks, Inc.), which could be completed in 10 minutes.

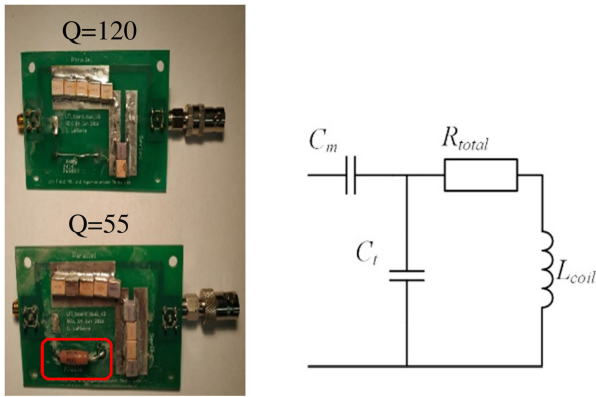


Fig. 4. Tuning and matching circuit boards (left) and corresponding circuit (right). The red rectangle (left) indicates the resistor used to adjust the Q of RF coil.



Fig. 5. Head-shaped liquid filled phantom. This phantom was filled with an aqueous solution of 9% NaCl and 1% Gd in DI.

### III. ANALYSIS

The quality factor of a RF coil used for receive relates to its passband and SNR and in this work, imaging experiments were performed to examine the relation between the quality factor and the imaging results. Moreover, with the goal of further improving the performance of RF coil, we also analyzed the relationship between RF coil performance and the design requirements in liner programing.

#### A. Quality Factor

According to equation (4), the bandwidth of a RF coil is affected by its quality factor Q. MRI experiments at 6.5 mT were performed to show how the quality factor Q affect the imaging result. The Q of the RF coil was adjusted by adding a resistor in series with the RF coil. Two tuning and matching circuit boards were made with Q of 55 and 120 respectively. The tuning and matching circuit and circuit boards was shown as Fig. 4. The RF coil used in this experiment is a uniformly wound spiral RF coil, reported in [3], which was shown as Fig. 11(a) in this work.

We scanned a head-shaped phantom filled by an aqueous solution of 9% NaCl, and 1% gadolinium in DI, shown as Fig. 5. A 3D b-SSFP sequence was used, with the second phase encode direction (i.e., the partition direction) along in the Z direction, a 50% undersampling ratio, matrix size of  $75 \times 64 \times 15$ , pixel size of  $2.5 \times 3.5 \times 8.5 \text{ mm}^3$ , the number of averages of 20 and the scan time was  $\sim 4$  minutes. Fig. 6 shows the images obtained with the spiral RF coil with different Q. Fig. 7 shows the plot

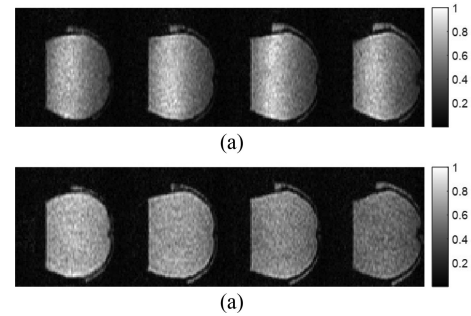


Fig. 6. Images obtained with the uniformly-wound spiral RF coil. (a) the image obtained by RF coil with  $Q = 120$ ; (b) the image obtained by RF coil with  $Q = 55$ . The horizontal axis is the readout dimension.

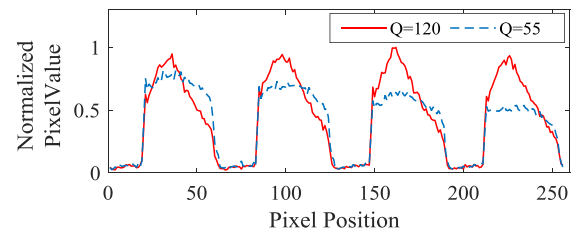


Fig. 7. The pixel values along the readout dimension in the images shown in Fig. 6.

which shows the pixel value on midline (perpendicular to Z axis in Fig. 6) of the images in Fig. 6. A very bright central region along the frequency encode direction is clearly visible in Fig. 6 from the high Q. This can also be seen in the plot in Fig. 7, the pixel value of images obtained with high Q RF coil has a sharp peak on each slice, which demonstrates that high Q RF coil has a narrower bandwidth.

The frequency encoding bandwidth of this experiment is 4.6 kHz; the Larmor frequency at 6.5 mT is 276 kHz; according to equation (4), the Q of the RF coil should be no greater than 60. A Q higher than 60 would narrow the bandwidth, whereas a Q lower than 60 will broaden the coil bandwidth. Therefore, a RF coil with Q lower than 60 would avoid the coil bandwidth problem. However, according to (3), (4) and (5), the lower the Q, the lower the SNR of RF coil. Thus, one should maintain the Q of a RF coil as high as possible provided it meets the readout bandwidth constraint; in this work, the Q of RF coil should be adjusted to 60 which could be implemented with a resistor in series with the coil windings.

#### B. Parameter Optimization

Linear programing was used to obtain an optimized coil winding pattern with required RF magnetic-field strength and homogeneity. In order to further optimize the winding pattern of RF coil to improve its performance, we studied the relationship between the design requirements ( $B_{1r}$  and  $\delta_1$ ) and the performance of RF coil.

We implemented linear programing with different  $B_{1r}$  and  $\delta_1$ . Fig. 8(a), (b) shows the results, obtained with  $\delta_1$  of 25% and the  $B_{1r}$  from 0.12 mT to 0.44 mT, where the 3D bar chart in



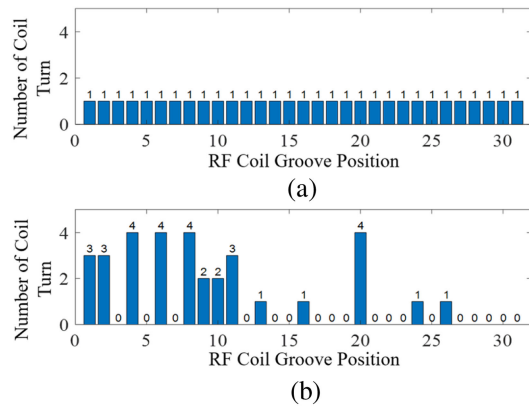


Fig. 10. RF coil pattern. (a) the coil pattern of the uniformly spiral RF coil; (b) the coil pattern of the optimal RF coil, which was obtained using linear programming with  $\delta_1$  of 25% and  $B1_r$  of 0.20 mT.

( $B1_r$ ) because an increase in the homogeneity requirement of RF magnetic field ( $\delta_1$ ) leads to a reduction in the SNR of optimized RF coil. The SNR of the uniformly wound spiral RF coil is higher than that of all optimized RF coils, however, the inhomogeneity  $\delta_2$  of the uniformly wound spiral RF coil, calculated with (12), is 65.60%.

$$\delta_2 = \frac{\max(B1_0) - \min(B1_0)}{\max(B1_0) + \min(B1_0)} \quad (12)$$

Where  $B1_0$  denotes the magnetic field component along  $z$  direction at target points,  $\max(B1_0)$  denotes the maximum effective component of the RF magnetic field, and  $\min(B1_0)$  denotes the minimum.

#### IV. RESULTS

In this work, we chose to design an optimized RF coil prototype with a target  $\delta_1$  of 25%; we empirically found that this value is very near the smallest value for which the optimization reliably converges. According to the SNR results shown in Fig. 9, the RF coil pattern obtained with  $B1_r$  of 0.2 mT was chosen because it has relatively high SNR and short wire length which make it simple to fabricate, tune and match, yet still has good performance. The number of turns in each groove position is shown as Fig. 10, and Fig 10(a) and (b) show that of the uniformly wound RF coil and the optimal RF coil. The Q of the uniformly wound RF coil and optimal RF coil are 55 and 58, respectively, with (normalized) SNR values of 1 and 0.68, respectively.

The coil pattern and photograph of the uniformly wound RF coil are shown in Fig. 11(a), and the 3D model and photograph of the optimized RF coil is shown in Fig. 11(b). We compared the optimal RF coil and the uniformly wound RF coil using the FEM simulation, and the magnetic field maps over the ROI in the  $y$ - $z$  plane are plotted in Fig. 12, and the magnetic field along the  $z$  axis is plotted in Fig. 13. Both figures indicate that the magnetic field produced by the optimized RF coil is more homogeneous over the ROI.

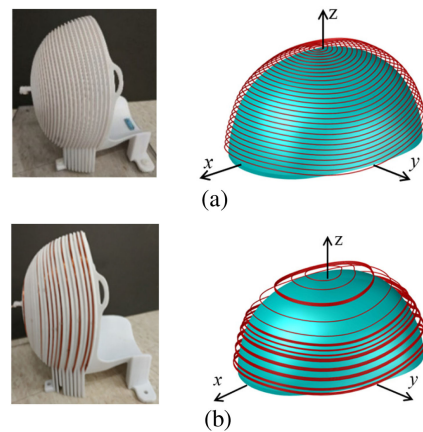


Fig. 11. The prototype and 3D model of RF coil. (a) the prototype (left) and 3D model (right) of the uniform wound RF coil; (b) the prototype (left) and 3D model (right) of the optimal wound RF coil.

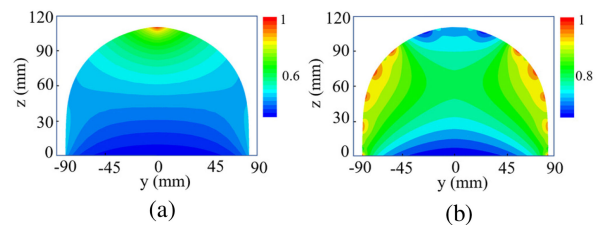


Fig. 12. Magnetic field maps. (a) the magnetic field map produced by the uniformly wound RF coil; (b) the magnetic field map produced by the optimal wound RF coil.

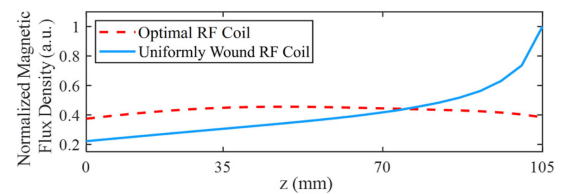


Fig. 13. Magnetic field component along the Z axis, produced by the uniformly wound RF coil and the optimized RF coil.



Fig. 14. Head-shaped structured phantom and internal structure.

Errors in the realization of RF coil, introduced by coil winding and head-shaped former processing, are inevitable; according to error analysis implemented by FEM simulation, the effect of realization error on magnetic field strength and homogeneity is less than 2%.

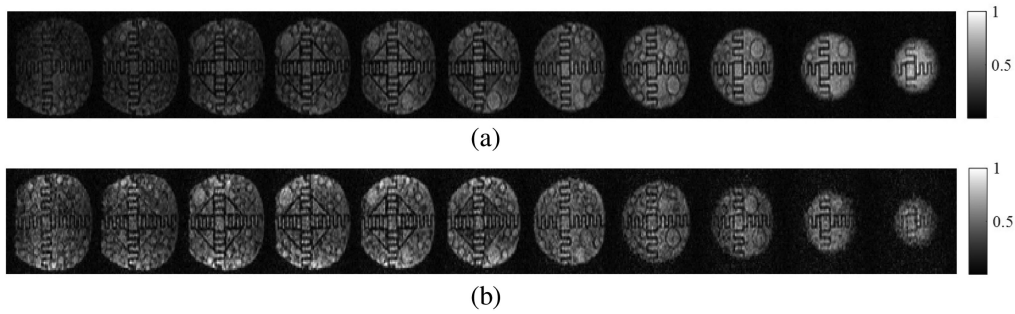


Fig. 15. MRI images of head-shaped phantom, where the number of averages is 20. (a) the images obtained with uniformly wound spiral RF coil; (b) the images obtained with optimized wound RF coil.

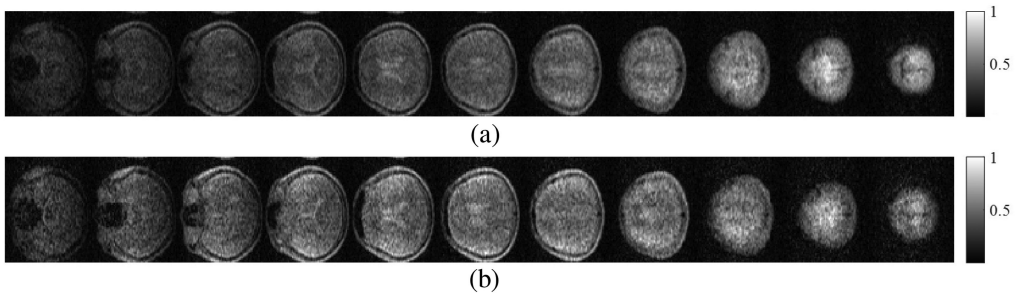


Fig. 16. MRI images of human brain, where the number of averages is 40. (a) the images obtained with the uniformly wound spiral RF coil; (b) the images obtained with optimized RF coil.

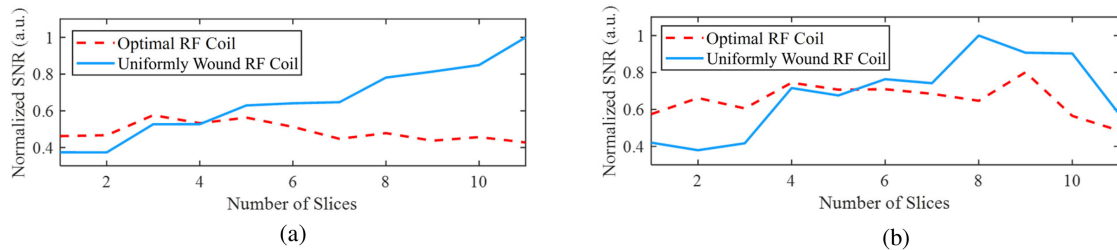


Fig. 17. Mean image SNR per slice for the (a) phantom images, and the (b) human brain images.

Both the uniformly wound RF coil and the optimized RF coil were used to scan a structured head-shaped phantom in our ULF MRI scanner operating at 6.5 mT (276 kHz). The phantom (Fig. 14) contains an internal structure and is filled by deionized water and balls of various sizes filled with  $\text{CuSO}_4$  solution with varying concentrations. A 3D b-SSFP sequence was used, with the partition direction along Z direction, a 50% undersampling ratio, matrix size of  $75 \times 64 \times 15$ , pixel size of  $2.5 \times 3.5 \times 8.5$  mm<sup>3</sup>, the number of averages of 20 and the scan time was  $\sim 4$  minutes. The performance of the optimized coil was compared to that of the uniformly wound RF coil. All the imaging parameters, the receiver gain and shim set values were kept constant between experiments and coils. The raw data was then reconstructed by applying the conventional 3D inverse fast Fourier Transform. Fig. 15 shows the comparison of the imaging results obtained by these 2 coils on a 6.5 mT MRI system which is described

in [3].

$$\text{Noise} = \sqrt{\left(\sum_{i=1}^{50} x_i^2\right) / 50} \quad (13)$$

The SNR of each slice is calculated by taking the ratio of the calculated signal and noise. The signal was calculated as the maximum of a moving average of 10-pixel values in the slice. For the noise, 50-pixel values,  $x_i$ , at the edge of slice were chosen, and the noise was calculated as (13). The calculation result was shown as Fig. 17(a). The variation of the SNR along  $z$  axis is similar to that of the magnetic field distribution; the SNR of all slices obtained with optimal RF coil have less variation between slices compared to the uniformly wound RF coil, however, the

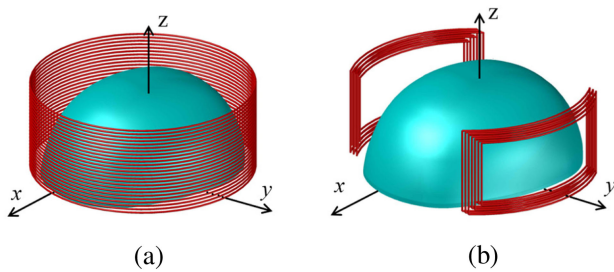


Fig. 18. Simulation Models. (a) the simulation model of a solenoid RF coil; (b) the simulation model of a saddle-style RF coil.

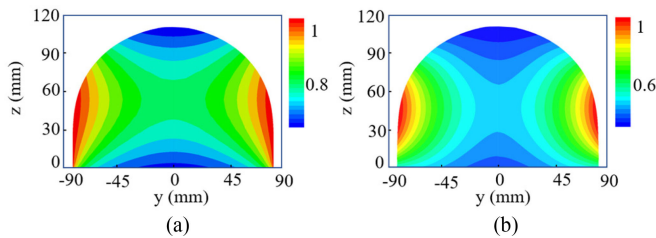


Fig. 19. Magnetic field map. (a) the magnetic field map produced by the solenoid in 18(a); (b) the magnetic field map produced by the saddle coil in 18(b).

TABLE I  
THE PARAMETERS OF RF COIL

	$Bl_{av}$ (mT)	Mean SNR	Inhomogeneity
Uniformly wound RF coil	0.166	1	65.60%
Optimal RF coil	0.202	0.68	24.32%
Solenoid RF coil	0.164	0.55	26.71%
Saddle RF coil	0.056	0.19	65.68%

SNR of 7 slices obtained by optimal wound RF coil is lower than that of the uniformly wound RF coil.

We also performed imaging of human heads, with the configuration of the scanner is as same as that in head-shaped phantom scanning, except that the number of averages was changed to 40, and imaging time is  $\sim 9$  minutes. The imaging results are shown in Fig. 16; the SNR of the images is shown as Fig. 17(b).

## V. DISCUSSION

Volume coils are generally preferred in brain imaging, and include solenoid- and saddle geometries. Our experience at 6.5 mT has led us to focus on the close-fitting head-shaped coils described above, however by way of completeness, we compare the performance of solenoid and saddle coils for ULF head imaging with FEM simulation. The simulation models are shown as Fig. 18. To enable a fair comparison, the inductance of the RF coil under study was adjusted in the FEM simulation to be as close as that of optimized RF coil, i.e.,  $164.5 \mu\text{H}$ . For the simulation, inductance of the solenoid RF coil is  $160.4 \mu\text{H}$  and the inductance of saddle RF coil is  $160.1 \mu\text{H}$ . The magnetic field maps of solenoid and saddle RF coils are plotted in Fig. 19. Table I compares the performance parameters of all the RF coils, including the uniformly wound and optimized coils, with

the mean SNR value over the ROI indicated calculated using equation (2). Among these classes of coils, we find that the magnetic field homogeneity and the SNR attainable with the optimized RF coil exceeds the best-fitting solenoid RF coil and saddle RF coils.

In this work, we have developed a novel hybrid method consisting of FEM simulation and linear programming to optimize a head-shape RF coil with the goal of obtaining an optimal result with high homogeneity and SNR. We find an intrinsic compromise must be made between SNR and homogeneity in RF coil optimization; an optimized RF coil with high SNR has low homogeneity, and one with high homogeneity has low SNR.

The hybrid optimization method was implemented with precondition that the position and shape of every loop making up of RF coil was pre-determined. In this work, the loop shape and position were determined according to the shape of human head, the direction of the static magnetic field of the MRI scanner, and the gauge of wire winding RF coil. All the loops are closely fitting to the head which distribute on the surface of a head-shaped former; the magnetization direction of each loop is perpendicular to the direction of the static magnetic field; and the gap between each coil is larger than the wire gauge. Our approach for determining the coil groove positions on the surface of a former picked according to the requirements of specific application is via optimization of the target parameters. This method could be extended to the design of the former geometry itself, but this approach needs further study.

In the analysis, the Q of the RF coil is a critical parameter. In low-field MRI, the Q of the RF coil was determined simply by the lumped circuit parameters (the so-called ‘‘Johnson noise regime’’) as opposed to the situation at high field where the RF coil Q includes factors from both the lumped circuit parameters as well as the body-noise of the subject under study (the ‘‘body noise’’ regime.) This arises because eddy current losses in the human body are strongly frequency dependent and virtually non-existent at 276 kHz.

In our analysis, we found that the performance of an optimized winding depends strongly on the requirements: to obtain an optimal RF coil in this regime, the requirements ( $Bl_r$  and  $\delta_l$ ) should be also studied in the optimization.

## VI. CONCLUSION AND FUTURE WORK

We have described a hybrid method consisting of FEM simulation and linear programming which provides a new approach for the design and optimization of complex wound coils. We studied the modified solenoid RF coil with the hybrid method, and find that the requirement of high homogeneity and the high SNR are somewhat contradictory. This means we have to compromise between these two performance parameters in RF coil optimization. We also scanned head-shaped phantoms and human heads at 6.5 mT to study the performance of the RF coil; the images obtained on the 6.5 mT MRI scanner also provide an example of the kind of improved performance attainable using optimized designs on an ultra-low-field MRI system.

Future work includes application of the hybrid optimization approach to head-shaped nested quadrature coils developed in

our laboratory for use at ULF. We also feel that the optimization method described here could also provide a way to optimized saddle RF coil, birdcage RF coil and even array RF coils.

## REFERENCES

- [1] L. L. Wald *et al.*, "Low-cost and portable MRI," *J. Magn. Reson. Imag.*, vol. 4, no. 3, p. 31, Oct. 2019.
- [2] S. Geethanath and J. T. Vaughan, "Accessible magnetic resonance imaging: A review," *J. Magn. Reson. Imag.*, vol. 49, no. 7, pp. e65–e77, Jan. 2019.
- [3] J. P. Marques, F. F. J. Simonis, and A. G. Webb, "Low-field MRI: An MR physics perspective," *J. Magn. Reson. Imag.*, vol. 58, Jan. 2019, Art. no. 1182.
- [4] D. Ma *et al.*, "Magnetic resonance fingerprinting," *Nature*, vol. 495, pp. 187–192, 2013.
- [5] B. Zhu *et al.*, "Image reconstruction by domain-transform manifold learning," *Nature*, vol. 555, no. 7697, pp. 487–492, Mar. 2018.
- [6] M. Sarracanie *et al.*, "Low-cost high-performance MRI," *Sci. Rep.*, vol. 5, no. 1, Oct. 2015, Art. no. 15177.
- [7] A. J. Mäkinen, K. C. J. Zevenhoven, and R. J. Ilmoniemi, "Automatic spatial calibration of ultra-low-field MRI for high-accuracy hybrid MEG–MRI," *IEEE Trans. Med. Imag.*, vol. 38, no. 6, pp. 1317–1327, Jun. 2019.
- [8] J. Tropp, "The theory of the bird-cage resonator," *J. Magn. Reson. (1969)*, vol. 82, no. 1, pp. 51–62, 1989.
- [9] Y. Ha *et al.*, "Design and use of a folded four-ring double-tuned birdcage coil for rat brain sodium imaging at 9.4," *T. J. Magn. Reson.*, vol. 286, pp. 110–114, 2018.
- [10] J. Paška, M. Cloos, and G. Wiggins, "A rigid, stand-off hybrid dipole, and birdcage coil array for 7 T body imaging," *Magn. Reson. Medicine*, vol. 80, no. 2, pp. 822–832, 2018.
- [11] S. Su, M. Zou, and J. Murphy-Boesch, "Solenoidal array coils," *Magn. Reson. Medicine*, vol. 47, no. 4, pp. 794–799, 2002.
- [12] H. S. Lee *et al.*, "Development of a solenoid RF coil for animal imaging in 3 T high-magnetic-field MRI," *Scanning*, vol. 30, no. 5, pp. 419–425, 2008.
- [13] J. Jin, "Electromagnetics in magnetic resonance imaging," *IEEE Antennas Propag. Mag.*, vol. 40, no. 6, pp. 7–22, Dec. 1998.
- [14] B. Blasiak *et al.*, "An RF breast coil for 0.2T MRI," *Concepts Magn. Reson. Part B: Magn. Reson. Eng.*, vol. 46, no. 1, pp. 3–7, 2016.
- [15] A. Wright *et al.*, "Helmholtz-pair transmit coil with integrated receive array for high-resolution MRI of trabecular bone in the distal tibia at 7 T," *J. Magn. Reson.*, vol. 210, no. 1, pp. 113–122, 2011.
- [16] B. Sporrer *et al.*, "A fully integrated dual-groove on-coil CMOS receiver for array coils in 1.5–10.5 T MRI," *IEEE Trans. Biomed. Circuits Syst.*, vol. 11, no. 6, pp. 1245–1255, Dec. 2017.
- [17] N. Avdievich *et al.*, "SENSE imaging with a quadrature half-volume transverse electromagnetic (TEM) coil at 4T," *J. Magn. Reson. Imag.*, vol. 24, no. 4, pp. 934–938, 2006.
- [18] A. Homagk *et al.*, "An expandable catheter loop coil for intravascular MRI in larger blood vessels," *Magn. Reson. Medicine*, vol. 63, no. 2, pp. 517–523, 2010.
- [19] H. Xu, S. M. Conolly, and G. C. Scott, "Homogeneous magnet design using linear programming," *IEEE Trans. Magn.*, vol. 36, no. 2, pp. 476–483, Mar. 2000.
- [20] S. Wright and L. Wald, "Theory and application of array coils in MR spectroscopy," *NMR Biomedicine*, vol. 10, no. 8, pp. 394–410, 1997.
- [21] R. E. Bolz, D. Eng., CRC Handbook of Tables for Applied Engineering Science, 1973.